International Journal of Analytical, Experimental and Finite Element Analysis
Volume 13, Issue 2, June 2026, pp 69 - 87
https://doi.org/10.26706/ijaefea.13.2.20260404

Biomechanical Evaluation of Fractured Femoral Locking Plates Using Finite Element Analysis

Himanshu Tamrakar[1], Uttam Kumar Kar[2]

[1] Research Scholar, Mechanical Engineering Department, CCET, Bhilai-490026, Chhattisgarh,
[2] Assistant Professor, Mechanical Engineering Department, CCET, Bhilai-490026, Chhattisgarh,

*Correspondence: ukkar093 @gmail.com

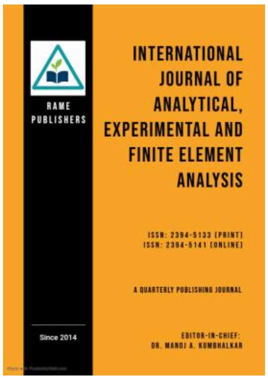

Article – Peer Reviewed
Received: 7 April 2026
Accepted: 15 June 2026
Published: 27 June 2026

Cite this article: Amarjeet Banjare, Uttam Kumar Kar, "Dynamic Analysis and ANN based Optimization of Thermally Stressed Rotating High-Pressure Compressor Blades", *International Journal of Analytical, Experimental and Finite Element Analysis*, RAME Publishers, vol. 13, issue 2, pp. 69-87, 2026.
https://doi.org/10.26706/ijaefea.13.2.20260404

Abstract: The femur is the longest and strongest bone in the human body and plays a critical role in load transfer between the hip and knee joints under physiological loading conditions. Femoral fractures are the most common orthopaedic injuries and often require internal fixation devices to restore structural stability and facilitate bone healing. The mechanical performance of the fixation system plays a crucial role in determining the success of fracture treatment. In the present study, a finite element-based biomechanical assessment of a fractured femur stabilized with a PMMA/Hydroxyapatite (PMMA/HA) composite locking plate was carried out under various physiological and impact loading conditions. A three-dimensional model of the fractured femur and locking plate assembly is developed from computer-aided design data and analyzed using finite element techniques. The PMMA/HA composite is selected as the plate material due to its favourable biocompatibility and potential for enhanced load transfer characteristics. Four loading scenarios are considered, namely joint loading during single-leg stance, trochanteric loading during single-leg stance, joint loading during fall, and trochanteric loading during fall. In addition, the biomechanical response of the fixation system is evaluated at four representative stages of the gait stance phase to investigate the influence of dynamic physiological loading.

The distributions of equivalent (Von-Mises) stress and total deformation were analyzed to assess the structural behavior of the bone-implant system. The results revealed that loading location and loading intensity significantly affect stress concentration and deformation patterns. Fall loading generated substantially higher stresses and deformations than normal stance loading, identifying it as the most critical condition for implant safety. Among the investigated loading cases, joint loading during fall produced the highest equivalent stress, whereas trochanteric loading during fall resulted in the largest deformation. The gait analysis further demonstrated that stress and deformation vary throughout the stance phase, with the highest values occurring during the terminal stance stage. A progressive shift of stress concentration from the medial to the lateral side of the femur was also observed during the gait cycle.

The findings indicate that the PMMA/HA composite locking plate provides effective fracture stabilization and satisfactory load-bearing capability under both physiological and impact loading conditions. The study contributes to the understanding of the biomechanical behavior of composite orthopaedic implants and offers useful insights for the design and optimization of next-generation femoral fracture fixation systems.

Keywords: Femur bone, Locking plate, PMMA, Gait loading, Finite element analysis, Stress distribution, Orthopaedic implant biomechanics.

The primary function of bone, as an organ is the structural support of the complete system of the body. It can be assumed that bone has a mechanical function in the body, in the same sense that a beam has a mechanical function in a building.

1.1 Overview of Femur bone

Femur bone is longest as well as strongest bone in human body and it is only bone in the thigh. It is situated between hip and knee. Anatomy of femur bone is shown in Fig. 1.

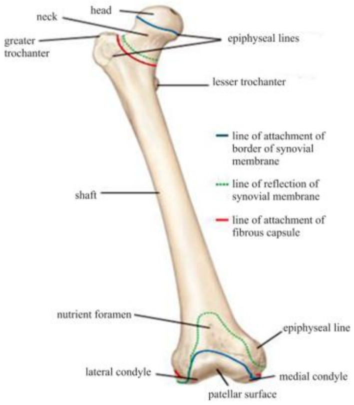

Figure 1. Anatomy of Femur bone

The long part of the bone is called the shaft. The top of the femur is part of the hip joint. The lower part of the femur is the knee joint. During static loading condition femur supports maximum weight of the body in between knee and hip joint.

1.2 Fractures in Femur bone

Femur fractures vary greatly, depending on the force that causes the break. The pieces of bone may line up correctly (stable fracture) or be out of alignment (displaced fracture). The skin around the fracture may be intact (closed fracture) or the bone may puncture the skin (open fracture).

Doctors describe fractures to each other using classification systems. Femur fractures are classified depending on: The location of the fracture (the femoral shaft is divided into thirds: distal, middle, proximal) The pattern of the fracture (for example, the bone can break in different directions, such as crosswise, lengthwise, or in the middle) Whether the skin and muscle over the bone is torn by the injury.

The most common types of femoral shaft fractures include Transverse fracture. In this type of fracture, the break is a straight horizontal line going across the femoral shaft. Oblique fracture. This type of fracture has an angled line across the shaft. Spiral fracture. The fracture line encircles the shaft like the stripes on a candy cane. A twisting force to the thigh causes this type of fracture. Comminuted fracture. In this type of fracture, the bone has broken into three or more pieces. In most cases, the number of bone fragments corresponds with the amount of force needed to break the bone.

Open fracture. If a bone breaks in such a way that bone fragments stick out through the skin or a wound penetrates down to the broken bone, the fracture is called an open or compound fracture. Open fractures often involve much more damage to the surrounding muscles, tendons, and ligaments. They have a higher risk for complications especially infections and take a longer time to heal.

Proximal femur fractures are common in both younger as well as older people. In young and healthy people, the injury results from high impact force, where as in the older people, most of the fractures are due to osteoporosis, fall from stairs or from any height. These types of fracture causes more damage to the surrounding tissue, have less healing property, and are prone to infection. A femoral shaft fracture is a bone fracture that occurs in the femur. They are typically sustained in high-impact trauma, because large amount of force needed to break the bone. Femoral shaft fractures are common in the people of all age groups in India due to high impact trauma, low impact trauma and osteoporosis disease

1.3 Femur locking plate

Femoral shaft fractures can be corrected by using locking compression plates which is most preferable now. Proximal femur locking compression plates (PF-LCP) have superior biomechanical stability and durability due to which it gained popularity since their inception. Femoral locking plate with femur bone is shown in Fig. 2.

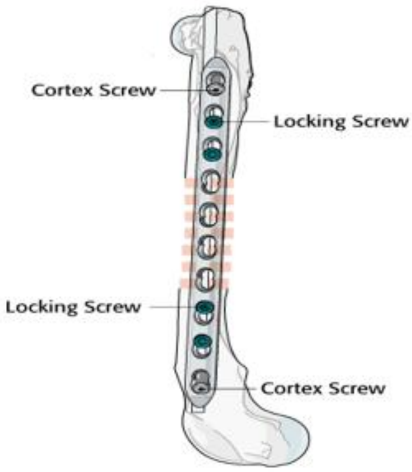

Figure 2. Femur bone with locking plate

The locking plate possesses several advantages in fracture fixation. It combines angular stability through locking screws with misalignment correction and fracture reduction into the plate by using suitable locking screw.

2. Literature Review

Femoral shaft and proximal femoral fractures constitute a significant orthopedic challenge due to the critical load-bearing function of the femur and its complex biomechanical characteristics. The increasing incidence of road traffic accidents, sports-related injuries, and osteoporosis-associated fractures has intensified the need for reliable and mechanically efficient fixation methods. Among the available internal fixation techniques, Locking Compression Plates (LCPs) have gained widespread acceptance because they provide enhanced stability, improved load distribution, and reduced risk of implant loosening and failure.

Numerous studies have investigated the biomechanical behavior, material selection, geometric design, and fixation stability of femoral locking plates using experimental techniques, analytical approaches, and finite element analysis (FEA). Factors such as plate material, plate thickness, screw configuration, screw–bone interaction, fracture pattern, and physiological loading conditions have been shown to significantly affect stress distribution, deformation characteristics, and fatigue performance of the implant. Recent research has also explored the dynamic response and vibration characteristics of bone–implant systems to better understand implant durability and long-term clinical outcomes.

The present literature survey critically reviews previous investigations related to the design, biomechanical performance, and optimization of femoral locking plate systems. Particular emphasis is placed on finite element modeling, material behavior, fixation stability, and stress analysis under physiological loading conditions. The review aims to identify existing research gaps and establish a foundation for the proposed study on the biomechanical analysis of fractured femoral locking plates.

Kraus et al. [1] employed micro-computed tomography (Micro-CT) to investigate gas formation and degradation behavior of magnesium fixation pins implanted in rat femora. Their study demonstrated the importance of evaluating implant biocompatibility and degradation mechanisms for orthopedic applications.

Fulkerson et al. [2] compared locking plate systems with conventional large-fragment plates secured using cables. Their experimental results revealed that locking plates exhibited superior axial compression and torsional strength. However, failure modes were more severe, particularly involving separation of the proximal femoral fragment.

Higgins et al. [3] evaluated the mechanical performance of locking plates and blade plates under axial compression and cyclic loading conditions. The authors reported that locking plate systems provided greater fixation strength and maintained stability regardless of bone quality. Their findings further supported the biomechanical advantages of locking plate fixation.

Vallier and Immler [4] conducted a retrospective clinical study comparing 95° blade plates and locking compression plates in the treatment of intra-articular and extra-articular femoral fractures. The study found significantly higher rates of complications, surgical revisions, and nonunion in patients treated with locking compression plates, highlighting the influence of clinical and surgical factors on implant performance.

Sahiti Lahari et al. [5] performed finite element analysis of the proximal femur for osteoporosis assessment. Using CT-image-based three-dimensional models developed in MIMICS and analyzed in ANSYS, they correlated finite element results with bone mineral density measurements obtained from dual-energy X-ray absorptiometry. The study demonstrated the effectiveness of FEA as a tool for evaluating bone strength and fracture risk.

Hassan et al. [6] analyzed the stress distribution and failure characteristics of the femur using finite element modeling. The maximum stress locations and critical failure loads were determined, providing valuable insights into the natural safety factors of bone structures and supporting the development of synthetic bone substitutes.

Pravat Kumar Satapathy et al. [7] investigated fractured femur fixation using a functionally graded bone plate through finite element analysis. The study revealed that replacing conventional titanium plates with functionally graded materials increased stress transfer at the fracture site by approximately 63% while reducing deformation by 15%, particularly under torsional loading conditions. These findings suggested improved load-sharing characteristics and enhanced fracture healing potential.

Macleod et al. [8] performed both experimental and numerical analyses to examine the influence of loading conditions on locking plate fixation systems. Their study demonstrated that loading methodology significantly affects construct stiffness, strain distribution within the bone, and stress concentration in the implant. The authors concluded that variations in reported stiffness values across previous studies could largely be attributed to differences in loading conditions.

Faris Tarlochan et al. [9] investigated the biomechanical design of composite femoral prostheses by examining the effects of stiffness, coating length, and interference press-fit. Their results indicated that a fully coated composite prosthesis with a 50 µm interference fit provided optimal load sharing, stress transfer, and reduced micromotion at the bone–implant interface.

Wisanuyotin et al. [10] evaluated six dual locking plate configurations for mid-shaft femoral fracture fixation using finite element analysis validated through cadaveric mechanical testing. The medial–lateral plate configuration exhibited the highest axial and bending stiffness, whereas the posterior–lateral configuration provided superior torsional stiffness. The close agreement between finite element predictions and experimental measurements confirmed the reliability of the numerical models.

Wang et al. [11] compared the biomechanical performance of Proximal Femoral Nail Antirotation (PFNA), Proximal Femoral Locking Plate (PFLP), and Less Invasive Stabilization System (LISS) implants for subtrochanteric femoral fractures using finite element analysis. For unstable fracture patterns, PFNA demonstrated superior fixation stability, lower implant stress, and reduced femoral head displacement. In contrast, PFLP and LISS provided comparable performance and improved stability in stable fracture configurations. The study emphasized the importance of selecting fixation methods according to fracture severity.

Pereira et al. [12] investigated the effects of near-cortical over-drilling on bone–plate construct performance through experimental testing and finite element analysis using rabbit femoral fracture models. The results showed that near-cortical over-drilling significantly increased load-bearing capacity while maintaining comparable bending stiffness. Finite element predictions closely matched experimental observations and revealed reduced stress concentration around the fixation region, suggesting improved conditions for fracture healing.

The reviewed literature demonstrates extensive research on femoral fracture fixation, implant materials, plate configurations, and finite element modeling techniques. However, limited studies have specifically investigated the biomechanical behavior of fractured femoral locking plates after implant damage or partial failure under realistic physiological loading conditions. Furthermore, the influence of plate fracture on stress concentration, deformation patterns, and structural integrity remains insufficiently explored. Therefore, a detailed finite element-based biomechanical analysis of fractured femoral locking plates subjected to physiological loading is required to better understand failure mechanisms and improve implant design and clinical outcomes.

3. Biomechanical Analysis of Cracked Femur bone

3.1 Geometric Modelling

Femur bone is obtained by surface modeling in AUTOCAD and locking plate and screw is obtained by CATIA software, whereas assembly of bone, plate & screw is obtained by using AUTOCAD software.

3.1.1 Locking plate

Locking plate is fracture fixation device with threaded screw holes, which allows screws to thread to the plate and can work as a fixed-angle device. This plate may have a mixture of holes that allow placement of both locking and traditional non locking screws. In this present work 6 holes locking plate is used which is shown in below fig. the dimensions of this plate is 125mm×12mm×2 mm. Diameter of cortical and locking hole is 4.5mm and 4mm respectively. This plate model is obtained by using CATIA software, which is shown in figure 3.

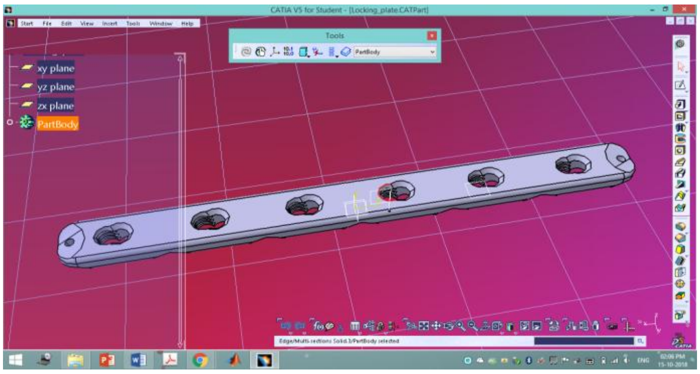

Figure 3. 3D model of locking plate

3.1.2 Femur bone

In this present work the femur bone is obtained by surface modeling using CATIA software. Obtained model is shown in below Fig. 4. Dimension of this femur bone is shown in Table 1.

Table 1. Dimensions of Femur bone

Dimensions	**Value (mm)**
Total length	450
Shaft length	350
Middle shaft diameter	25
Dia. Condylar and proximal portion	40

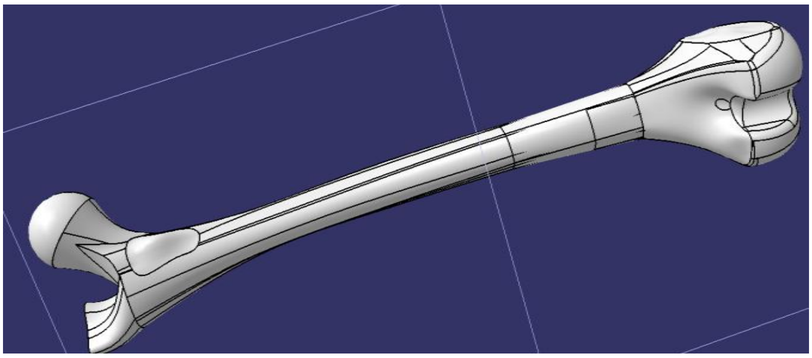

Figure 4. 3D model of Femur bone

3.1.3 Locking screw

Locking screw systems have advantages over the conventional screw systems. As the screws are tightened, they lock to the plate, thus stabilizing the segments without the need to compress the bone to the plate. At this present work locking screw is obtained by using CATIA software and the total length of this screw is 20mm, pitch is 1.75mm, major and minor diameter are 4mm & 3.5mm respectively. 3D model of screw with same dimensions is shown in Fig. 5.

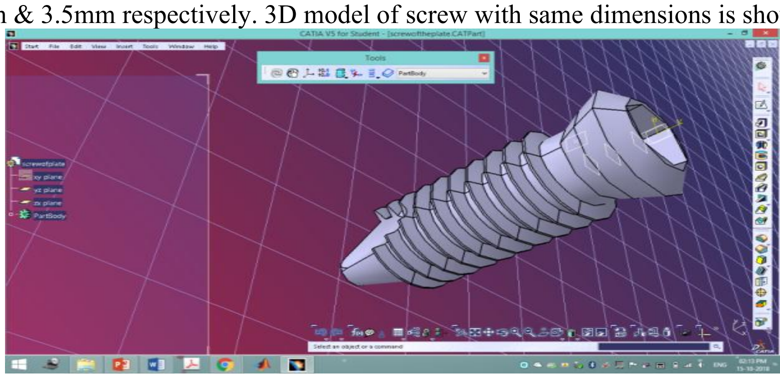

Figure 5. 3D model of locking screw

3.1.4 Cracked model of Femur bone

The assembly of femur bone, locking plate and locking screws is illustrated in Fig. 6. This assembly model is obtained by using AUTOCAD software. There is 15 mm cut in the shaft portion of the femur bone. Therefore it is a single cracked femur bone.

Figure 6. 3D model of assembled bone, plate & screw

3.2 Von-Mises failure criterion theory

Failure will occur in a material if the maximum distortion energy at a point due to given set of loads exceeds the maximum distortion Energy induced due to a uniaxial load at the Yield point. In this case, a material is said to start yielding when the Von-Mises Stress reaches a value known as yield strength, The Von-Mises stress is used to predict yielding of materials under complex loading from the results of uniaxial tensile tests.

$$\frac{1}{2}(\sigma_1^2 - \sigma_1\sigma_2 + \sigma_1^2) \leq S_{yp}^2 \quad (1)$$

With factor of safety

$$\frac{1}{2}(\sigma_1^2 - \sigma_1\sigma_2 + \sigma_1^2) \le \left(\frac{S_{yp}}{FOS}\right)^2 \tag{2}$$

We know that

Total distortion energy per unit volume =Difference of Total strain energy per unit volume and hydrostatic strain energy per unit volume

$$U_d = U - U_V \tag{3a}$$

But total strain energy is

$$U = \frac{1}{2E}[\sigma_1^2 + \sigma_2^2 + \sigma_3^2 - 2\vartheta(\sigma_1\sigma_2 + \sigma_2\sigma_3 + \sigma_3\sigma_1)] \tag{3b}$$

And Hydrostatic strain energy

$$U_v = \frac{1-2\vartheta}{E}[\sigma_1^2 + \sigma_2^2 + \sigma_3^2 + 2(\sigma_1\sigma_2 + \sigma_2\sigma_3 + \sigma_3\sigma_1)] \tag{4}$$

$$U = \frac{1}{2E}[\sigma_1^2 + \sigma_2^2 + \sigma_3^2 - 2\vartheta(\sigma_1\sigma_2 + \sigma_2\sigma_3 + \sigma_3\sigma_1)] \tag{5a}$$

$$U_v = \frac{1-2\vartheta}{6E}[\sigma_1^2 + \sigma_2^2 + \sigma_3^2 + 2(\sigma_1\sigma_2 + \sigma_2\sigma_3 + \sigma_3\sigma_1)] \tag{5b}$$

Subtitling for U and U_V in $U_d = U - U_V$ yields

$$U_d = \left(\frac{1+\vartheta}{E}\right)[(\sigma_1^2 + \sigma_2^2 + \sigma_3^2) - (\sigma_1\sigma_2 + \sigma_2\sigma_3 + \sigma_3\sigma_1)] \tag{6a}$$

$$U_d = \left(\frac{1+\vartheta}{6E}\right)[((\sigma_1 - \sigma_2)^2 + (\sigma_2 - \sigma_3)^2 + (\sigma_3 - \sigma_1)^2)] \tag{6b}$$

When yielding occurs in simple tension test Principal stresses are

$$\sigma_1 = S_y, \sigma_2 = 0 \tag{7}$$

Substituting an expression for distortion energy

$$U_d = \left(\frac{1+\vartheta}{6E}\right)[\left((S_y - 0)^2 + (0-0)^2 + (0 - S_y)^2\right)] \tag{8a}$$

$$U_d = \left(\frac{1+\vartheta}{6E}\right)[2S_y^2] \tag{8b}$$

$$(\sigma_1 - \sigma_2)^2 + (\sigma_2 - \sigma_3)^2 + (\sigma_3 - \sigma_1)^2 = 2S_y^2 \tag{9}$$

$$\sqrt{\left(\frac{(\sigma_1 - \sigma_2)^2 + (\sigma_2 - \sigma_3)^2 + (\sigma_3 - \sigma_1)^2}{2}\right)} = S_Y \tag{10}$$

3.3 Mesh Generation

Mesh generation is the practice of generating a polygonal or polyhedral mesh that approximates a geometric domain. Three dimensional meshes created for finite element analysis need to consist of tetrahedral, pyramids, prisms or hexahedral. Meshing consist of following values-number of element = 55110 and number of nodes = 93608. Meshing structure of implanted femur bone is shown in figure 7.

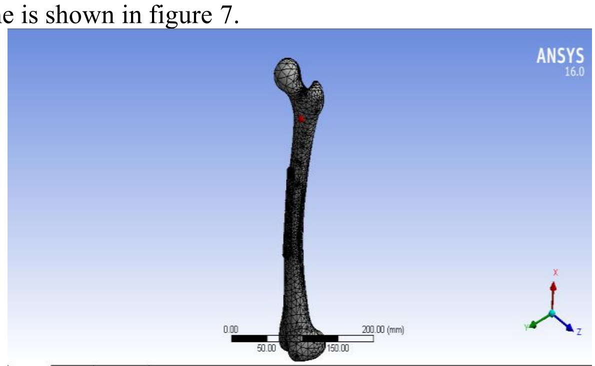

Figure 7. Meshing of Femur bone

The properties of different materials are shown in Table 2.

Table 2. Properties of different materials

Bone& prosthetic plate materials	Density Kg/m^3	Young's modulus (GPa)	Poisson ratio	Ultimate tensile strength (MPa)	Ultimate compressive strength (MPa)
Femur cortical bone	1750	16.7	0.3	43.44$\pm$3.62	115.29$\pm$12.94
PMMA/ HA	1180	220	0.2	47-79	83-124
Stainless steel 316L	7750	193	0.31	485	570
Ti-alloy(Ti-6AL-4V)	4500	120	0.32	993	1086

For the analysis of femoral locking plate with femur it is required to create a single crack which is shown in Fig. 8. Considering 10 mm single crack in the shaft portion of the femur bone.

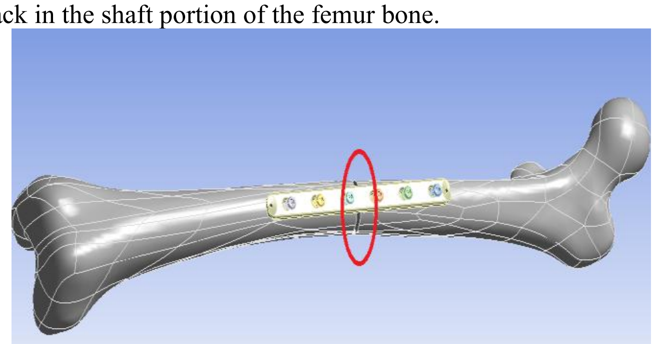

Figure 8. Single cracked implanted Femur bone

4. Considering only weight of an adult body with stable condition

4.1.1 Boundary conditions

1) Applied force of 75kg (750N) will act in downward x-direction in this case, because it is assumed that average weight of an adult person nearly comes in defined weight in femur head in downward direction by selecting circular area which is shown in above Fig. 9.
2) Fixed support in tibia or bottom portion of the femur bone by selecting all the faces in bottom end of the femur bone.

Assuming 1. Deflection in y & z direction is zero in proximal head side.($u_y = 0$, & $u_z = 0$)

2. Deflection in x-direction is zero in condylar side.($v_x = 0$)

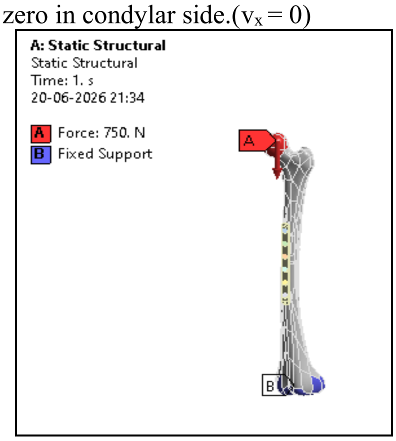

Figure 9. Boundary condition for analysis

4.1.2 Validation Study

Figure 10 present the total deformation and equivalent stress obtained for the stainless-steel femoral locking plate. The numerical results show close agreement with the values reported by Ajay Dhanopia et al.[15], thereby validating the accuracy of the present finite element model.

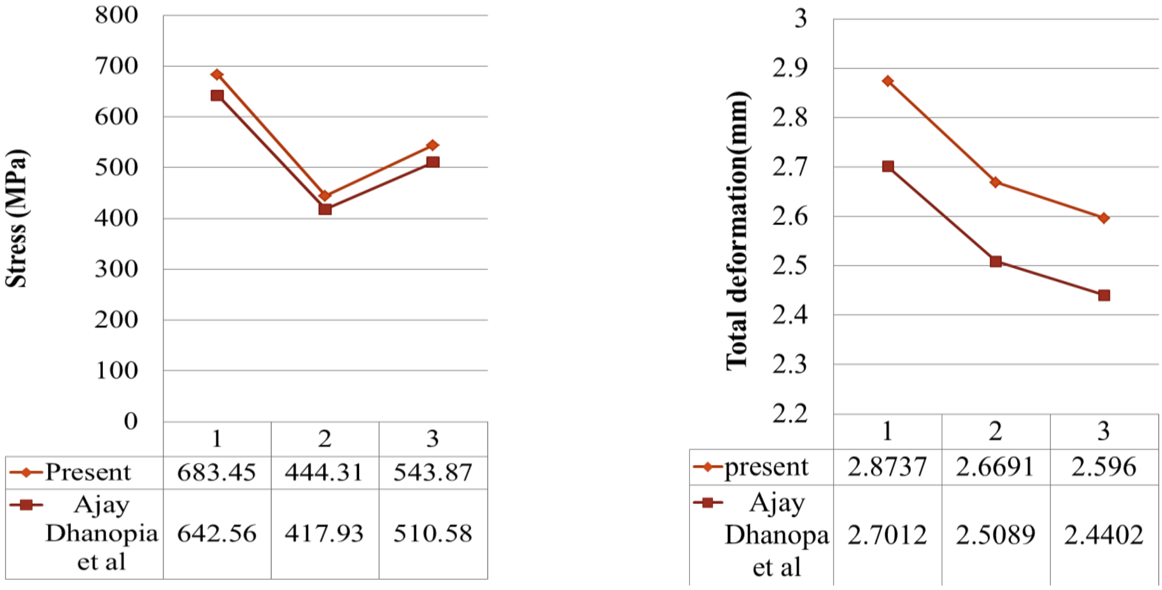

Figure 10 Comparison of Equivalent stress and total deformation of Femoral locking plate

Minor variations between the two sets of results are observed, which can be attributed to differences in geometric modeling and boundary conditions. In the present study, the femur bone and femoral locking plate geometries were developed using CATIA software, resulting in slight differences in the model configuration compared to the reference study. Nevertheless, the overall trend and magnitude of deformation and stress remain consistent, confirming the reliability and effectiveness of the proposed finite element analysis.

4.3 Numerical Results

Fig. 11 (a–f) illustrates the total deformation and equivalent (von Mises) stress distributions in the femoral locking plate–bone assembly for Stainless Steel, Ti-alloy, and PMMA/HA composite materials when only body weight is considered. The deformation contours reveal that the PMMA/HA composite plate exhibits the lowest deformation among the investigated materials, indicating enhanced structural stiffness and improved resistance to displacement at the fracture site. The Ti-alloy plate shows moderate deformation, whereas the Stainless Steel plate experiences comparatively higher deformation. The von Mises stress distributions indicate that the PMMA/HA composite develops the highest stress levels, followed by the Ti-alloy and Stainless Steel plates. The increased stress observed in the PMMA/HA composite suggests that a larger portion of the applied load is carried by the implant, resulting in improved load-bearing capability.

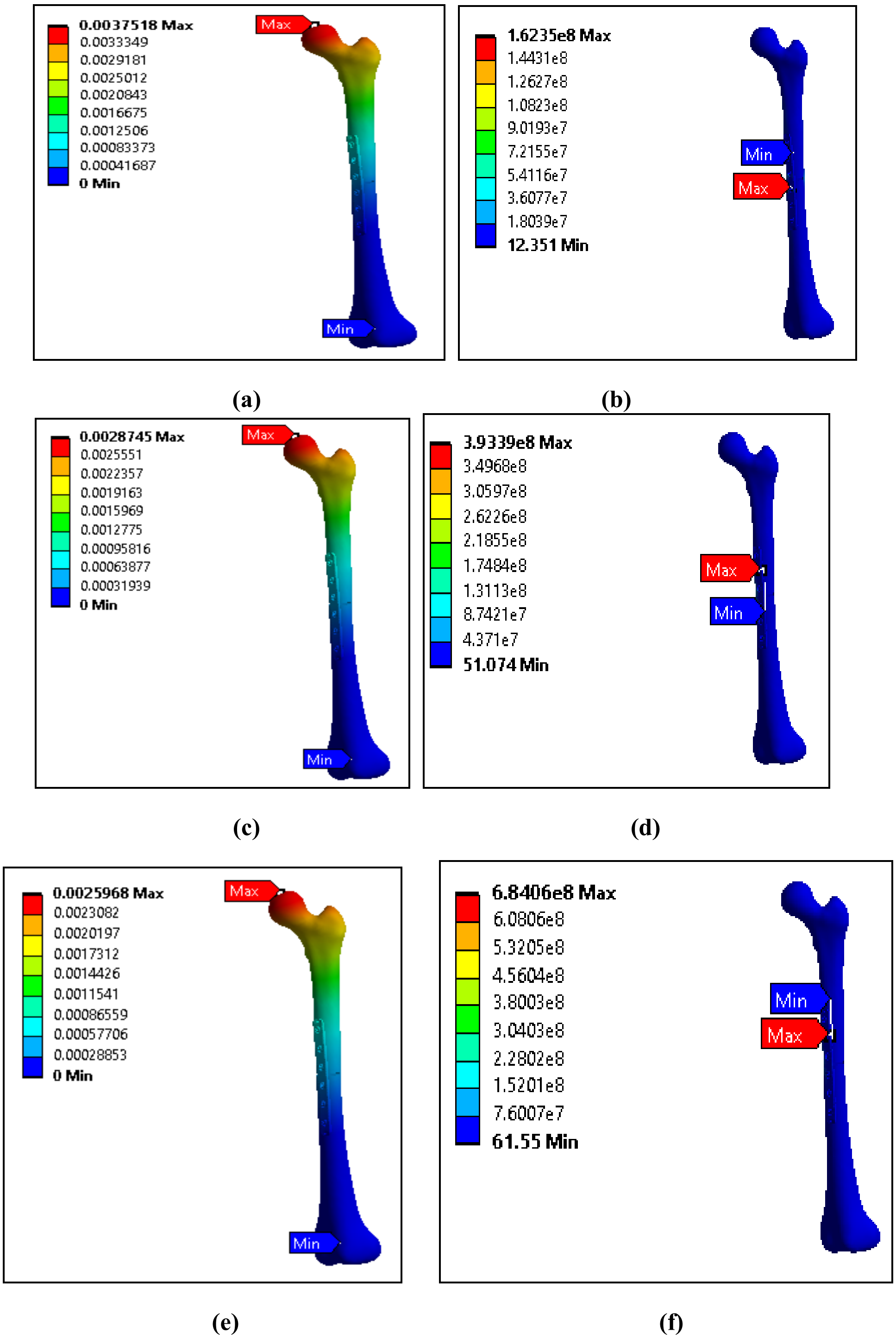

Figure 11. Deformation and Stress distribution of Femoral locking plate at different material consideration (a-b) Stainless Steel (c-d) Ti-alloy (e-f) PMMA/HA composite

Although the stress magnitude is higher, it remains within the permissible strength limits of the composite material, indicating safe operation under the applied loading conditions. The stress concentrations for all three materials are primarily observed around the screw holes and near the fracture region, which is consistent with the transfer of load between the plate and bone. The PMMA/HA composite demonstrates a more effective load-transfer mechanism while maintaining lower deformation, which is beneficial for fracture stabilization and minimizing interfragmentary motion. In contrast, the metallic plates exhibit lower stress levels but comparatively higher deformation, indicating a different load-sharing behavior between the implant and the bone.

Overall, the PMMA/HA composite exhibits superior mechanical performance by providing enhanced fixation stability with minimal deformation while sustaining acceptable stress levels. These characteristics make the PMMA/HA composite a promising alternative to conventional metallic locking plates for femoral fracture fixation applications.

4.4 Analysis of Femur locking plate at single leg stance and falling condition

4.4.1 Loading conditions

i. Fixed support in tibia or bottom portion of the femur bone by selecting all the faces in bottom end of the femur bone.
ii. To analyze biomechanical behavior of implanted femur two loading conditions are considered. Condition 1- single-legged stance phase of gait, taken from literature . In all daily activities stance phase of the gait cycle is seen very often, like stair climbing, stair descending, running ,walking and jogging; this is the main reason to consider single legged stance as a basic and important loading condition . The load direction in the single leg stance case is shown in Figure 12 (a-b).

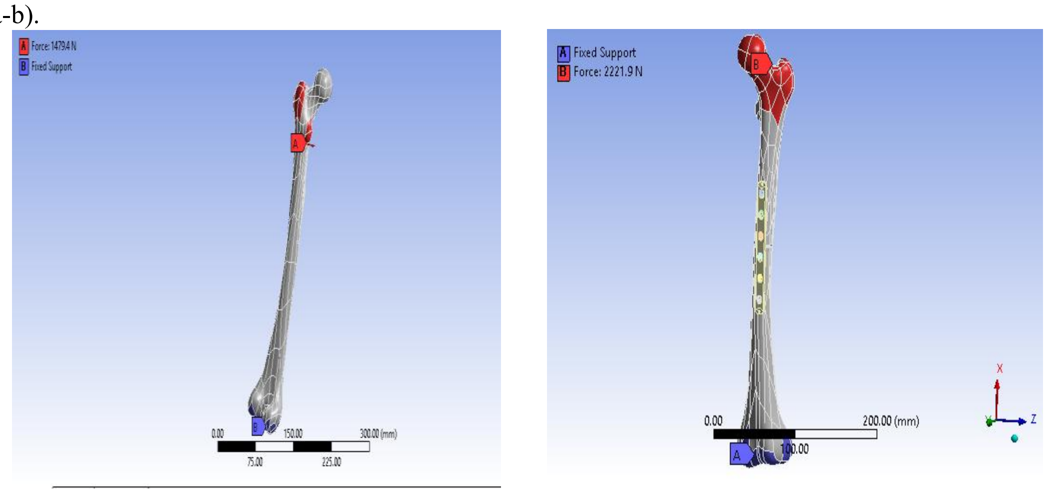

(a) At joint (b) At Trochanter

Figure 12. Forces Acting on the Hip Joint During Single-Leg Standing

iii. At a specific period every muscle is active in the gait cycle. The muscle which is active in single-legged stance phase of gait is the Gluteus Medias. The muscular and joint contact resultant forces are applied on two different locations. The muscular load created by the Gluteus Medias muscle is applied on the great trochanter area and joint contact force is applied on the femoral head. The direction of two forces are opposite with an angle to the femoral shaft.
iv. Load condition 2 represents impact of falling on the femur from standing position. The direction of loads to replicate impact from a fall is a medially directed load applied to the great trochanteric and an equal and opposite laterally directed load applied to the femoral head. The load direction in the single leg stance case is shown in Fig. 13 (a-b).

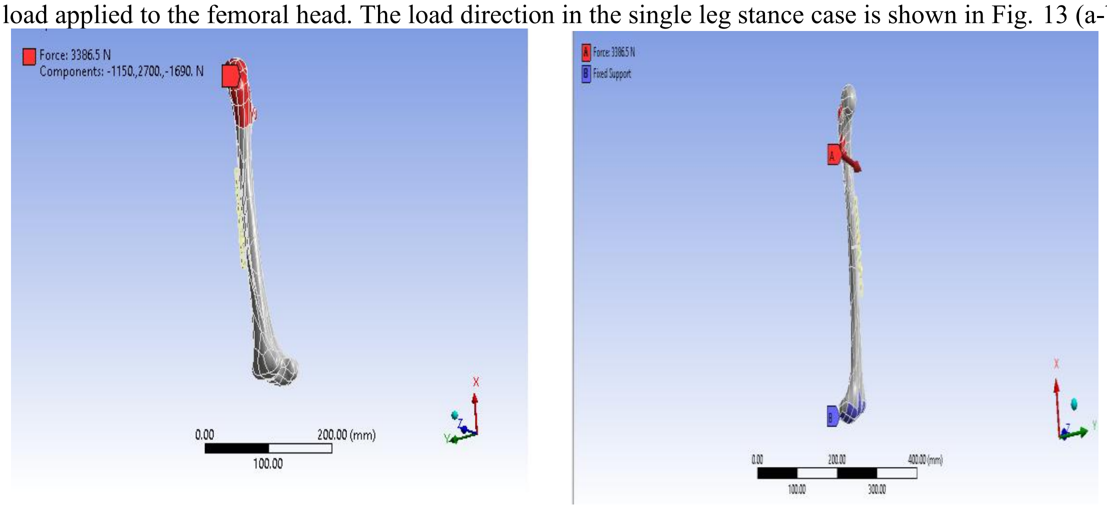

(a) At joint (b) At Trochanter

Figure 13. Forces Acting on the Hip Joint During fall

v. In this work, a global Cartesian axis set is defined with a x- axis parallel to the long axis of the femur shaft and implant plate, the x- axis along the anterial to posterial of the femur and the y-axis in medial to lateral directions. The magnitude and direction of loadings are listed in Table 3.

Table 3. Magnitude and direction of loadings[2]

Conditions		**Direction of loads**		
Stance phase*		A-P	M-L	S-I
1	Joint	211	453	2165
2	Trochanter	195	485	-1384
Impact from fall*				
3	Joint	1690	-2700	1150
4	Trochanter	-1690	2700	-1150

4.4.2 Stress–Deformation response of fractured femur bone under physiological joint load

Fig. 14 (a-d) presents the equivalent stresses obtained for the fractured femur stabilized with a PMMA/HA composite femoral locking plate under four different loading scenarios. Conditions 1 and 2 correspond to single-legged stance loading applied at the hip joint and greater trochanter, respectively, whereas Conditions 3 and 4 represent fall-induced loading applied at the hip joint and greater trochanter, respectively. The results indicate that the loading condition significantly influences the stress distribution and deformation behavior of the fixation system. Under single-legged stance loading, the equivalent stress increases from 372.89 MPa in Condition 1 to 654.27 MPa in Condition 2, demonstrating that load application at the greater trochanter generates higher localized stresses compared to the physiological joint load.

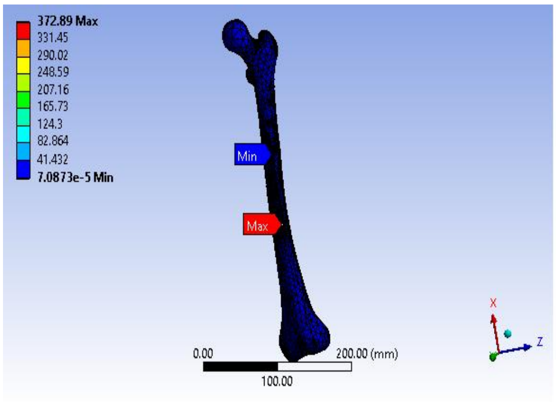

(a) Condition 1

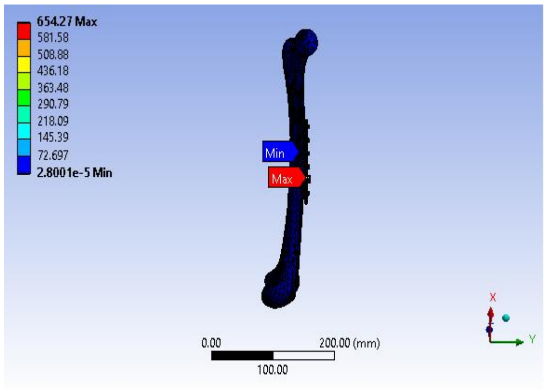

(b) Condition 2

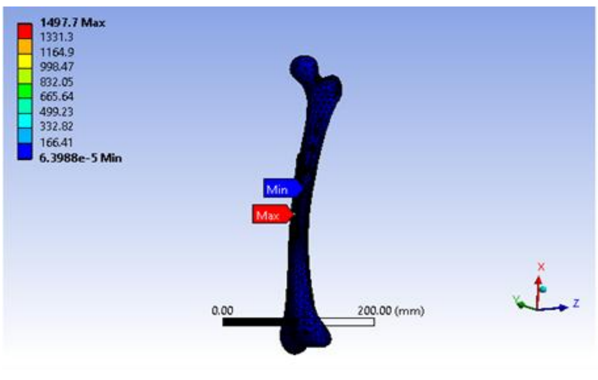

(c) Condition 3

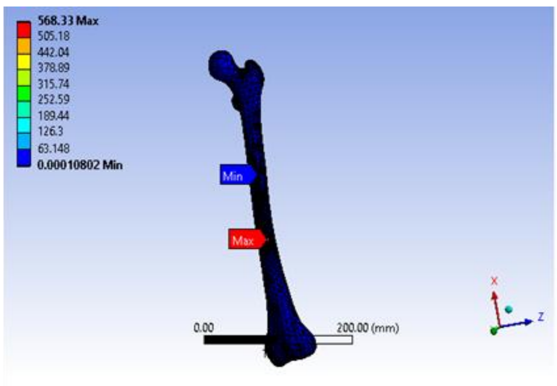

(d) Condition 4

Figure 14. Equivalent stress distribution on cracked femur bone

The corresponding deformation values as shown in Fig 15(a-b) are 2.72 mm and 1.79 mm, respectively, indicating that despite higher stresses, the trochanteric loading condition produces slightly lower displacement.

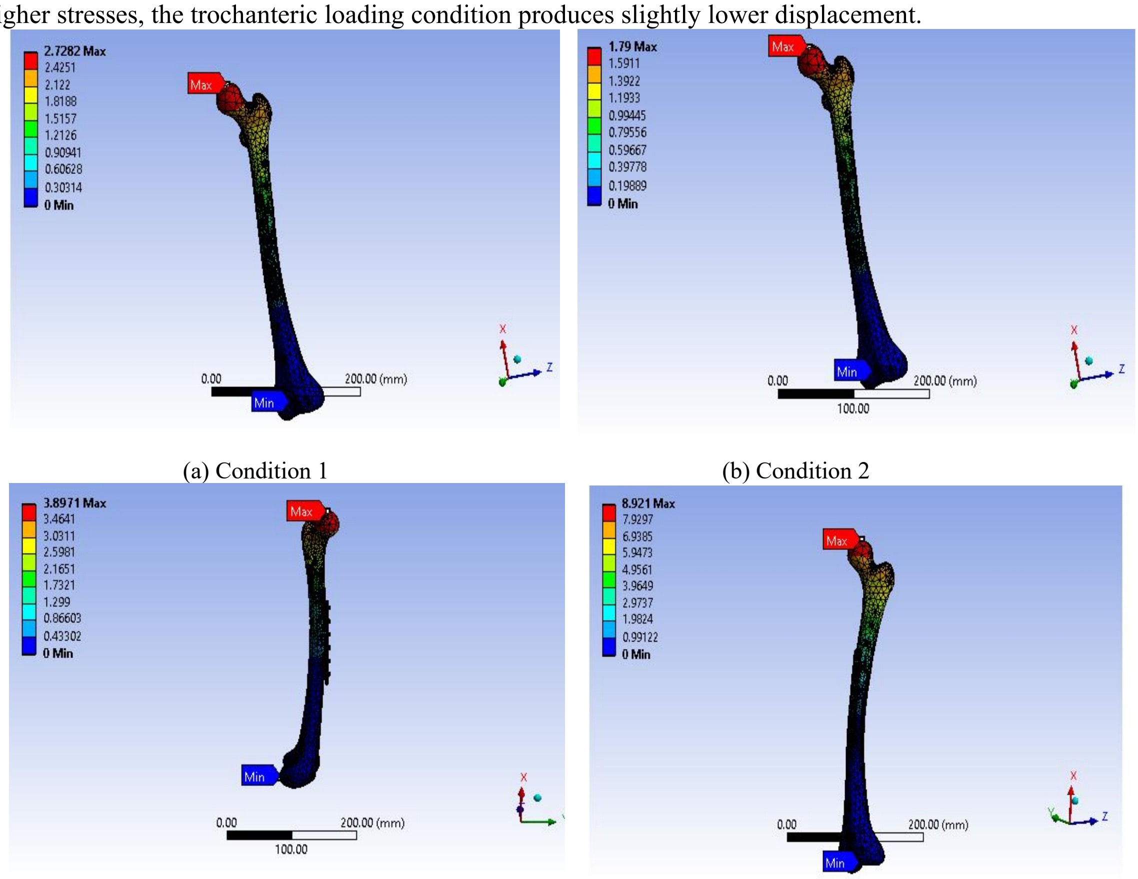

(a) Condition 1 (b) Condition 2

(c) Condition 3 (d) Condition 4

Figure 15. Total deformation of cracked femur bone

A substantial increase in stress is observed under fall loading conditions. Condition 3 (joint load during fall as shown in Fig. 15 (c) produces the highest equivalent stress of 1497.7 MPa and a deformation of 3.89 mm, indicating a severe mechanical response due to the high impact forces generated during a fall event. This suggests that fall-induced loading represents the most critical scenario for implant integrity and fracture stability. In contrast, Condition 4 (trochanteric load during fall as shown Fig 15 (d)) results in a lower equivalent stress of 568.33 MPa but exhibits the highest deformation of 8.92 mm, indicating greater structural displacement and potential instability of the fixation system.

The stress concentrations are primarily observed around the fracture region and screw-plate interfaces, where load transfer between the implant and bone is most significant. The PMMA/HA composite locking plate effectively distributes the applied loads while maintaining structural continuity across the fractured femur. However, the elevated stresses and deformations under fall conditions highlight the importance of considering accidental impact loads in the design and evaluation of orthopaedic fixation devices.

4.5 Analysis of femoral locking plate during stance phase of gait cycle

4.5.1 Gait events

From the stance phase of the gait, the data for the following four points are extracted: heel contact (ST1), loading response (ST2), mid-stance (ST3), and heel off (ST4). ST1 is set when the height of the heel marker at the heel of the foot is at the lowest point of the right heel contact in the position, this data is taken from the 3D motion analyzer, with a start and end points of a stride set as 0% and 100%, respectively. ST2 is set when the foot became flat with an anterior ground reaction force vector, moving up toward the hip (10% of the gait cycle). ST3 is set when the vertical axis was starting to be at the lowest; that is, when it passed the mid-foot, the foot became flat with the ankle neutral, and the ground reaction vector is minimally displaced from the joint center (15% of the gait cycle) and also ST 3 is set for the duration just before the vertical axis height of the heel marker rose. At this point, the ankle is dorsiflexed, and the vector is anterior to the knee and ankle (30% of the gait cycle). Finally, ST4 is set for the free forward fall of the body (50% of the gait cycle). The ground reaction force data are extracted from the four stages [10]. The magnitude of all the joint contact and muscle forces and directions are shown in Fig. 16.

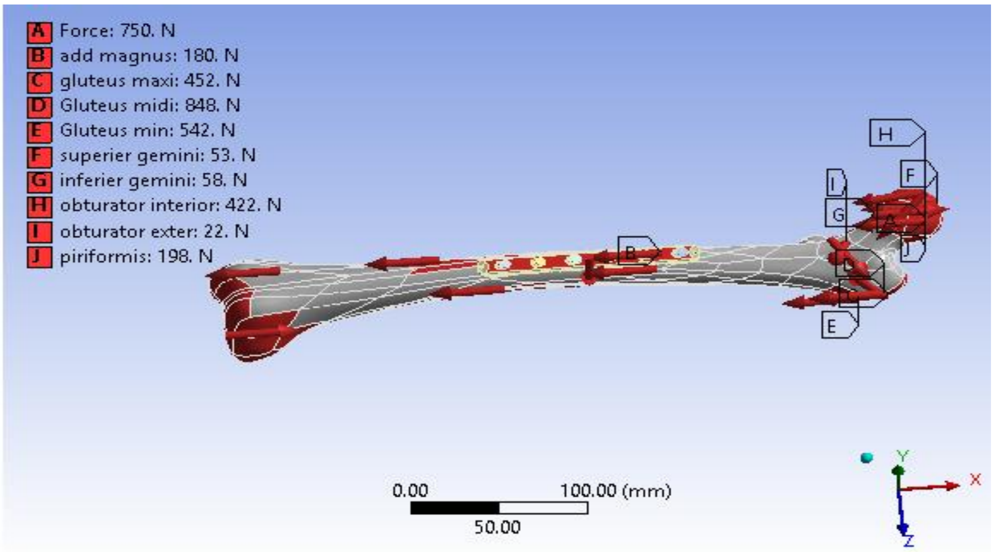

Figure 16 Muscle and joint contact forces

Considering a single crack in the shaft portion of the femur bone and locking plate with locking screw is attached. Material assigned for locking plate and screw is PMMA/2.5 % HA composite material which is suitable for human body. The finite element analysis is conducted by applying the muscle force and joint contact force calculated from the inverse dynamic musculoskeletal model simulation to the CT-image based right femur model. Magnitude and direction of different muscle and joint forces are given in Table 4.

Table 4. Muscle and hip joint contact forces at the subdivided stance phase of a gait event (N)

Gait Phase Muscle	Heel Contact (ST1)	Loading response (ST2),	mid-stance (ST3)	heel off (ST4)
Add Magnus	180	102	0	0
Gluteus maxi	452	432	406	389
Gluteus medi	848	862	840	853
Gluteus mini	542	563	516	582
Inferior gemeli	58	60	62	32
Superior gemeli	53	54	54	60
Obturatorexter	22	23	27	32
Obturator inter	422	410	404	435
Piriformis	198	192	180	193
Quadratusfemoris	25	23	17	28
Biceps femoris	185	155	115	165
Ten faslatae	24	18	14	9
Gastro-lateral	370	370	372	390
Gastro-medial	540	534	530	562
Vastuslateralis	13	12	11	7
Vastusmedialis	4	4	2	2
Vastusintermedius	8	6	2	5

Figure 16 shows the max Von-Mises stress and max Von-Mises strain at four stance phase stages. The area most influenced by the load moved from the medial part of the femur to the lateral part, starting from the ST3. Figure 27 and figure 28 shows the resulting max Von-Mises stress, max Von-Mises strain, and total deformation. The max Von-Mises stress, max Von-Mises strain, and total deformation are 225.73 MPa, 3.3505x10-2 mm/mm, and 18.878 mm, respectively at ST1; 260.24 MPa, 3.1022x10-2 mm/mm, and 18.796 mm at ST2; 254.88 MPa, 2.896x10-2mm/mm, and 18.148 mm at ST3; and 275.35 MPa, 3.3527x10-2 mm, and 19.796 mm at ST4. Thus, the max Von-Mises stress, max Von-Mises strain, and total deformation are highest at ST4 and lowest at ST3.

4.6.2 Biomechanical Response of the Fractured Femur

Figure 17 (a-d) illustrates the variation of equivalent (Von-Mises) stress in the fractured femur fixed with a PMMA/HA femoral locking plate during four representative stages of the stance phase, respectively. The results reveal that both the magnitude and location of stress concentration vary significantly throughout the gait cycle due to changes in load magnitude and direction.

A noticeable shift in the highly stressed region is observed from the medial side of the femur toward the lateral side beginning at ST3. This transition indicates a redistribution of load transfer within the bone-implant system as the body progresses through the stance phase. Such variations are attributed to the changing joint reaction forces and muscle forces acting on the femur during walking.

The maximum Von-Mises stress values obtained at ST1, ST2, ST3, and ST4 are 225.73 MPa, 260.24 MPa, 254.88 MPa, and 275.35 MPa, respectively.

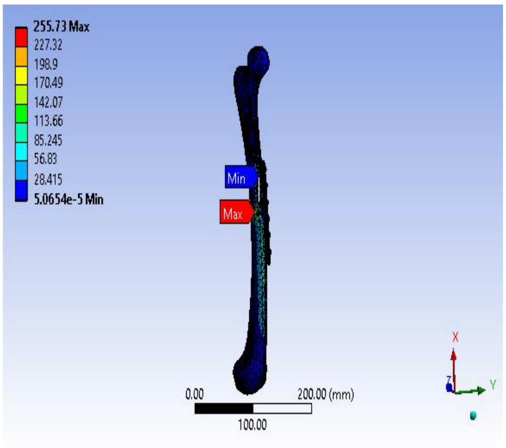

(a) Heel contact ST 1

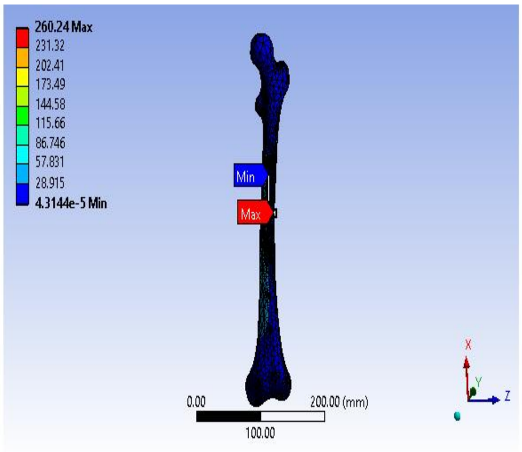

(b) Loading response ST 2

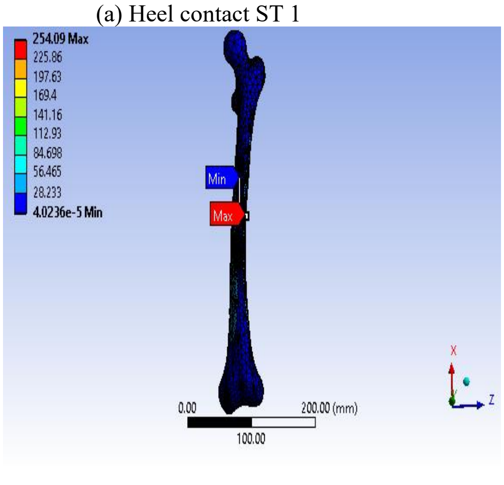

(c) Mid stance ST 3

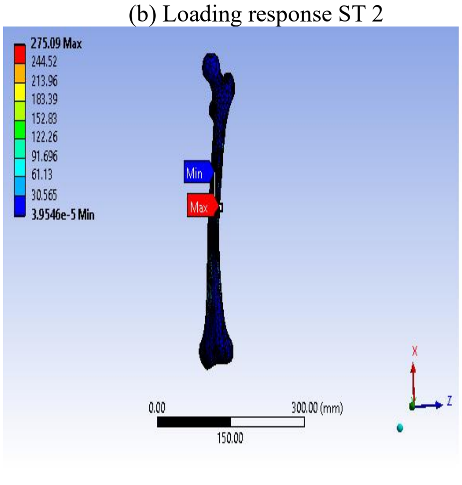

(d) Heel off ST 4

Figure 17 Von-Mises stress distribution on femur bone during gait cycle

Similarly, the corresponding total deformation values are 18.878 mm, 18.796 mm, 18.148 mm, and 19.796 mm shown in Fig 18 (a-b).

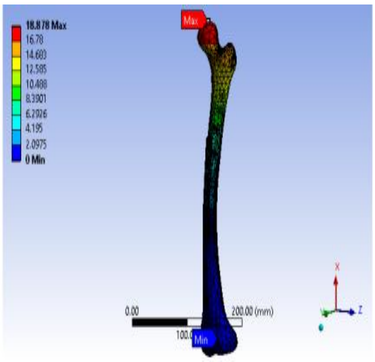

(a) Heel contact ST 1

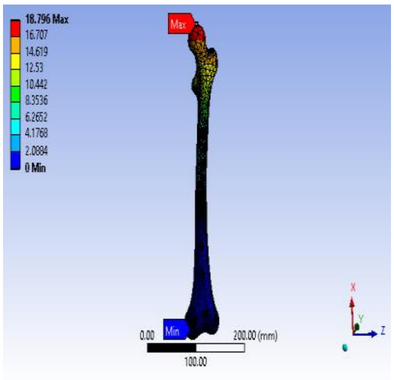

(b) Loading response ST 2

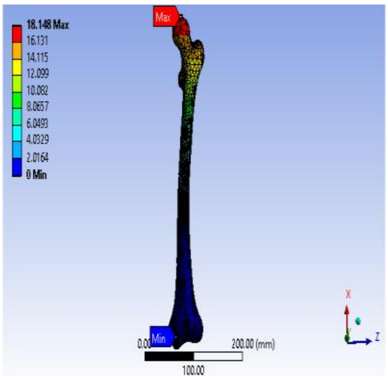

(c) Mid stance ST 3

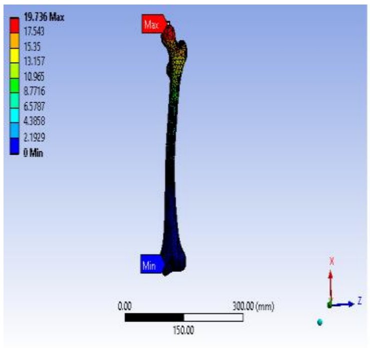

(d) Heel off ST 4

Figure 18. Structural deformation on femur bone during gait cycle

From Fig. 19(a-b), it is very clearly observed that among all loading stages, ST4 exhibits the highest stress and deformation, indicating that this stage imposes the most critical mechanical demand on the fixation system. The increased loading at ST4 may be associated with peak weight transfer and higher joint reaction forces during the terminal stance phase, resulting in greater stress concentration around the fracture and fixation regions.

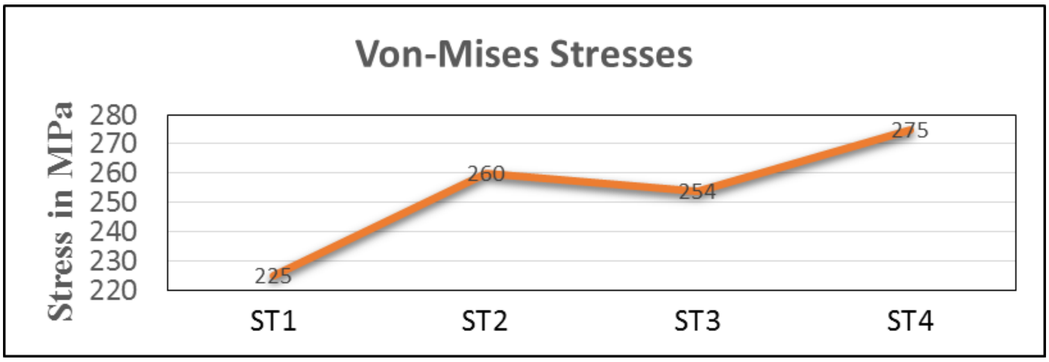

(a)

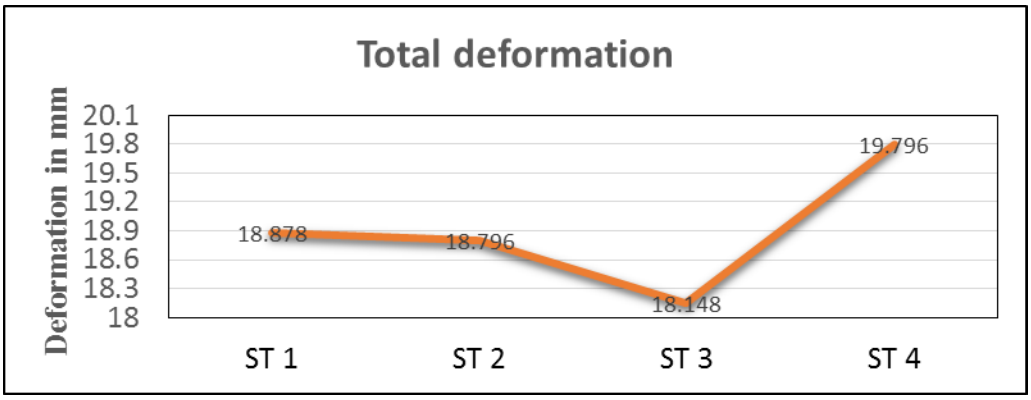

(b)

Figure 19. Magnitude of stress and deformation during gait cycle

Conversely, ST3 demonstrates the lowest deformation and relatively lower stress levels, suggesting a more favourable load-sharing condition between the PMMA/HA locking plate and the femoral bone. The reduced deformation at ST3 indicates improved structural stability and lower risk of excessive interfragmentary motion, which is beneficial for fracture healing.

The relatively small variation in stress between ST2 and ST3 indicates that the fixation system maintains consistent mechanical performance during the mid-stance period. However, the increase in stress and deformation at ST4 highlights the necessity of considering dynamic gait loading rather than relying solely on static loading conditions for implant evaluation. Failure to account for stance-phase variations may underestimate the peak stresses experienced by the implant during daily activities.

Overall, the PMMA/HA composite locking plate demonstrates stable biomechanical behavior throughout the gait cycle while effectively transferring physiological loads across the fractured femur. The findings emphasize that the terminal stance phase (ST4) represents the most critical condition for implant design and assessment due to the maximum stress and deformation developed during this stage.

5. Conclusion

The present study investigated the biomechanical behavior of a fractured femur stabilized with a PMMA/HA composite femoral locking plate under various physiological and impact loading conditions using finite element analysis. A three-dimensional femur-locking plate assembly was developed and analyzed to evaluate stress distribution and deformation characteristics under single-leg stance, fall loading, and different stages of the gait stance phase. The following conclusions are drawn from this study:

- The present study provide valuable insight into the design optimization of femoral locking plates with varying numbers of holes. Finite element analysis reveals that increasing the number of holes leads to a reduction in overall deformation under applied loading, indicating improved load redistribution along the plate. A comparative evaluation of PMMA and ZM21 magnesium alloy demonstrates that PMMA exhibits more uniform stress distribution and lower total deformation, which are critical factors for enhancing implant stability and minimizing stress shielding during fracture healing. Based on the mechanical performance observed, PMMA shows superior suitability compared to ZM21 magnesium alloy for femoral locking plate applications under static loading conditions.
- The results demonstrated that the loading magnitude and point of application significantly influence the mechanical response of the bone-implant system. Under single-leg stance loading, the fixation system exhibited comparatively lower stress and deformation, indicating adequate structural stability during normal daily activities. In contrast, fall loading generated substantially higher stress and deformation levels, identifying accidental falls as the most critical condition for implant performance and fracture stability.
- The analysis of four different loading scenarios revealed that the maximum equivalent stress occurred under joint loading during fall conditions, whereas the greatest deformation was observed under trochanteric loading during fall

conditions. These findings highlight the necessity of considering both physiological and impact loading cases while evaluating orthopaedic fixation devices.

- Furthermore, the gait-based stance-phase analysis demonstrated that stress and deformation vary throughout the walking cycle. The highest equivalent stress and deformation were observed during ST4, while the minimum deformation occurred during ST3. The stress concentration region was found to shift from the medial side to the lateral side of the femur as the stance phase progressed, indicating a dynamic redistribution of load within the bone-implant system.
- The PMMA/HA composite locking plate exhibited satisfactory load-bearing capability and fixation stability under all investigated loading conditions. The lower deformation and effective stress transfer characteristics indicate its potential as an alternative to conventional metallic implants for femoral fracture fixation. Overall, the study provides valuable insight into the biomechanical performance of composite orthopaedic implants and contributes to the development of safer and more efficient fracture fixation systems.

References

[1] Kraus et al . Social class, conceptualism, and empathic accuracy. Psychol Sci 2010;21:1716–21.

[2] Fulkerson et al. Biomechanics of locked plates and screws. J Orthop Trauma 2004;18:488–93.

[3] Hingins et al. Biomechanical comparison of dynamic condylar screw and locking compression plate fixation in unstable distal femoral fractures: An in vitro study. J Orthop Trauma 2013;47:615–20.

[4] Vallier and Immler. Comparison of the 95-degree angled blade plate and the locking condylar plate for the treatment of distal femoral fractures. J Orthop Trauma 2012:327–32.

[5] Lahari S, Al E. Finite Element Analysis of Femur in the Evaluation of Osteoporosis. J Pharm Biol Chem Sci 2011.

[6] Hassan Mehboob, Kim J, Mehboob A, Chang S-H. How post-operative rehabilitation exercises influence the healing process of radial bone shaft fractures fixed by a composite bone plate. Compos Struct 2017;159:307–15.

[7] Pravat Kumar Satapathy et al. Analysis of fractured femur bone with functionally graded bone plate at femur bone fracture site by adopting finite element method. IOP Conf Ser Mater Sci Eng 2018:330 01 2027.

[8] A.R.MacLeod, P Pankaj AS. Experimental and numerical investigation into the influence of loading conditions in biomechanical testing of locking plate fracture fixation devices. Bone Jt Res 2018;7:111–20.

[9] Tarlochan F, Mehboob H, Ali Mehboob, Chang S-H. Biomechanical design of a composite femoral prosthesis to investigate the effects of stiffness, coating length, and interference press fit. Compos Struct 2018;204:803–13.

[10] Wisanuyotin T, Sirichativapee W, Paholpak P, Kosuwan W, Kasai Y. Optimal configuration of a dual locking plate for femoral allograft or recycled autograft bone fixation: A finite element and biomechanical analysis. Clin Biomech 2020;80. https://doi.org/10.1016/j.clinbiomech.2020.105156.

[11] Wang J, Ma JX, Lu B, Bai HH, Wang Y, Ma XL. Comparative finite element analysis of three implants fixing stable and unstable subtrochanteric femoral fractures: Proximal Femoral Nail Antirotation (PFNA), Proximal Femoral Locking Plate (PFLP), and Reverse Less Invasive Stabilization System (LISS). Orthop Traumatol Surg Res 2020;106:95–101. https://doi.org/10.1016/j.otsr.2019.04.027.

[12] Pereira GJ, Rahal SC, Barboza WM, Moroz I, Leão AL, Alves MM, et al. Study of a near-cortical over-drilling technique on plate constructs with a conical locking system in a rabbit femoral fracture using a finite element model. Med Eng Phys 2025;144. https://doi.org/10.1016/j.medengphy.2025.104399.

[13] Uttam Kumar Kar, Bhushan RK. Design and analysis of femoral locking plate under different loading conditions using suitable material. Mater Today Proc 2020;21:1128–34.

[14] Iulian Antoniac , [1] Kraus *et al*., “Social class, conceptualism, and empathic accuracy,” *Psychological Science*, vol. 21, pp. 1716–1721, 2010.

[2] Fulkerson *et al*., “Biomechanics of locked plates and screws,” *Journal of Orthopaedic Trauma*, vol. 18, pp. 488–493, 2004.

[3] Hingins *et al*., “Biomechanical comparison of dynamic condylar screw and locking compression plate fixation in unstable distal femoral fractures: An in vitro study,” *Journal of Orthopaedic Trauma*, vol. 47, pp. 615–620, 2013.

[4] C. Vallier and W. Immler, “Comparison of the 95-degree angled blade plate and the locking condylar plate for the treatment of distal femoral fractures,” *Journal of Orthopaedic Trauma*, pp. 327–332, 2012.

[5] S. Lahari *et al*., “Finite element analysis of femur in the evaluation of osteoporosis,” *Journal of Pharmaceutical,*

Biological and Chemical Sciences, 2011.
[6] H. Mehboob, J. Kim, A. Mehboob, and S.-H. Chang, "How post-operative rehabilitation exercises influence the healing process of radial bone shaft fractures fixed by a composite bone plate," *Composite Structures*, vol. 159, pp. 307–315, 2017.
[7] P. K. Satapathy *et al*., "Analysis of fractured femur bone with functionally graded bone plate at femur bone fracture site by adopting finite element method," *IOP Conference Series: Materials Science and Engineering*, vol. 330, Art. no. 012027, 2018.
[8] A. R. MacLeod, P. Pankaj, and A. S. Simpson, "Experimental and numerical investigation into the influence of loading conditions in biomechanical testing of locking plate fracture fixation devices," *Bone & Joint Research*, vol. 7, pp. 111–120, 2018.
[9] F. Tarlochan, H. Mehboob, A. Mehboob, and S.-H. Chang, "Biomechanical design of a composite femoral prosthesis to investigate the effects of stiffness, coating length, and interference press fit," *Composite Structures*, vol. 204, pp. 803–813, 2018.
[10] T. Wisanuyotin, W. Sirichativapee, P. Paholpak, W. Kosuwan, and Y. Kasai, "Optimal configuration of a dual locking plate for femoral allograft or recycled autograft bone fixation: A finite element and biomechanical analysis," *Clinical Biomechanics*, vol. 80, Art. no. 105156, 2020, doi: 10.1016/j.clinbiomech.2020.105156.
[11] J. Wang, J.-X. Ma, B. Lu, H.-H. Bai, Y. Wang, and X.-L. Ma, "Comparative finite element analysis of three implants fixing stable and unstable subtrochanteric femoral fractures: Proximal Femoral Nail Antirotation (PFNA), Proximal Femoral Locking Plate (PFLP), and Reverse Less Invasive Stabilization System (LISS)," *Orthopaedics & Traumatology: Surgery & Research*, vol. 106, pp. 95–101, 2020, doi: 10.1016/j.otsr.2019.04.027.
[12] G. J. Pereira, S. C. Rahal, W. M. Barboza, I. Moroz, A. L. Leão, M. M. Alves, *et al*., "Study of a near-cortical over-drilling technique on plate constructs with a conical locking system in a rabbit femoral fracture using a finite element model," *Medical Engineering & Physics*, vol. 144, Art. no. 104399, 2025, doi: 10.1016/j.medengphy.2025.104399.
[13] U. K. Kar and R. K. Bhushan, "Design and analysis of femoral locking plate under different loading conditions using suitable material," *Materials Today: Proceedings*, vol. 21, pp. 1128–1134, 2020.
[14] I. Antoniac, M. Miculescu, V. M. Păltânea, A. S. P. H. Q. G. P. A. R., and K. E. (author name as available), "Magnesium-based alloys used in orthopedic surgery," *Materials*, vol. 15, Art. no. 1148, 2022.
[15] A. Dhanopia and M. Bhargava, "Finite element analysis of human fractured femur bone implantation with PMMA thermoplastic prosthetic plate," *Procedia Engineering*, vol. 173, pp. 1658–1665, 2017, doi: 10.1016/j.proeng.2016.12.190.
Marian Miculescu VM (Păltânea) ASPHQGPAR andKamel E. Magnesium-Based Alloys Used in Orthopedic Surgery. Materials (Basel) 2022;15:1148.
[15] Dhanopia A, Bhargava M. Finite Element Analysis of Human Fractured Femur Bone Implantation with PMMA Thermoplastic Prosthetic Plate. Procedia Eng 2017;173:1658–65. https://doi.org/10.1016/j.proeng.2016.12.190.